Available online at www.sciencedirect.com
ScienceDirect
International Journal of Solids and Structures 44 (2007) 8424–8439
INTERNATIONAL JOURNAL OF SOLIDS AND STRUCTURES
www.elsevier.com/locate/ijsolstr

An asymptotically correct classical model for smart beams

Sitikantha Roy, Wenbin Yu *, Dong Han

Department of Mechanical and Aerospace Engineering, Utah State University, Logan, UT 80322-4130, USA

Received 9 February 2007; received in revised form 8 May 2007
Available online 06 July 2007

Abstract

An asymptotically correct classical beam model has been developed for smart slender structures using the variational asymptotic method. Taking advantage of the slenderness of the structure, we asymptotically split the original three-dimensional electromechanical problem into a two-dimensional electromechanical cross-sectional analysis and a one-dimensional beam analysis. The one-dimensional beam analysis could be geometrically nonlinear or linear depending whether the original three-dimensional analysis is geometrically nonlinear or linear. The cross-sectional analysis, implemented using the finite element method, provides an asymptotically correct, one-dimensional constitutive model for smart slender structures without a priori assumptions regarding the geometry of the cross section, the distribution of the electric field, and the location of smart materials, such as embedded or surface mounted. Several examples are used to validate the accuracy of the present theory with available results in the literature and three-dimensional commercial finite element packages.

Keywords: Variational asymptotic method; Smart beams; VABS

1. Introduction

In recent years, there has been a strong interest in applying active materials to make structures "smart" (Chopra, 2002; Chee et al., 1998; Saravanos and Heyliger, 1999). Active materials such as piezoelectrics are capable of sensing and reacting to external stimuli and thus provide a new dimension for us to improve the performance of modern and future structural systems (Noor et al., 2000). Despite tremendous advances in the technology of smart-structures, the analytical predictive capabilities for smart structures are still very limited in comparison to those for conventional composite structures. Many engineering structures can be analyzed using beam models if one dimension is much larger than the other two dimensions of the structure. For this very reason, such structures are usually termed as smart beams. To take advantage of this geometrical feature, different researchers have proposed various smart beam models to capture the behavior associated with the two small dimensions eliminated in the final one-dimensional (1D) beam analysis.

* Corresponding author. Tel.: +1 4357978246; fax: +1 4357972417.
E-mail address: wenbin.yu@usu.edu (W. Yu).
URL: http://www.mae.usu.edu/faculty/wenbin (W. Yu).

0020-7683/$ - see front matter
doi:10.1016/j.ijsolstr.2007.06.028

Generally speaking, most of the studies in the literature can be classified as engineering models which are based on a priori kinematic assumptions, asymptotic models which are derived based on asymptotic expansions of the three-dimensional (3D) quantities, and models based on the Saint–Venant principle.

Engineering models begin with assuming some kind of distribution through the cross section for the 3D quantities in terms of the 1D quantities defined on a chosen beam axis. These models dominate the literature on the modeling of smart beams. They can be further classified as uncoupled models (Crawley et al., 1990; Robbins and Reddy, 1991; Park et al., 1996; Zhang and Sun, 1996; Smyser and Chandrashekhara, 1997) if only actuation of smart materials is treated, or coupled models (Saravanos and Heyliger, 1995; Raja et al., 2000) if both actuation and sensing capabilities of smart materials are treated simultaneously in the modeling process. These models use assumptions mainly based on engineering intuition and have clear physical meaning. The numerical implementation of such models can be developed straightforwardly from a variational statement. However, most of the a priori kinematic assumptions are natural extensions from those for homogeneous, isotropic beams and cannot be easily justified for heterogeneous structures made with anisotropic materials such as smart beams. Moreover, there is no rational way for the analysts to determine the loss of accuracy and what kind of assumptions (i.e., single-layer versus layerwise, first-order versus higher-order) should be used for sufficient accuracy while keeping a reasonable computational cost.

Unlike engineering models, asymptotic models reduce the original 3D problem into a sequence of 1D beam models by taking advantage of the small parameters inherent in the structure (Altay and Dokmeci, 2003). The conventional practice is to apply a formal asymptotic expansion directly to the system of governing differential equations of the 3D problem and successively solve the 1D field equations from the leading order to higher orders. Although these models are mathematically elegant and rigorous, sometime it is difficult to interpret the physical meanings of certain terms at a particular order level, and it is very difficult, to implement these theories numerically. These methods become intractable for a complex problem such as smart beams. Although there are some conventional asymptotic models for smart plates developed (Reddy and Cheng, 2001), such models for smart beams are rarely developed.

The variational asymptotic method (VAM) introduced by Berdichevsky (1979) can be used to construct beam models with both merits of engineering models (viz., systematic and easy numerical implementation) and asymptotic models (viz., without a priori kinematic assumptions) (Yu et al., 2002). Recently, Cesnik et al. applied VAM to model smart beams with active twist using active fiber composites. They have developed classical models for smart thin-walled beams (Cesnik et al., 2001), smart solid beams (Cesnik and Ortega-Morales, 2001), and refined models for smart solid beams (Cesnik and Palacios, 2003; Palacios and Cesnik, 2005). All these models have been implemented in the computer code UM/VABS. Using the temperature analogy, the effects of smart materials were initially modeled by assuming a constant and known electric field inside the active material (Cesnik et al., 2001; Cesnik and Ortega-Morales, 2001; Cesnik and Palacios, 2003). Later in Palacios and Cesnik (2005), a coupled analysis has been carried out using a modal procedure that allows arbitrary definition of 1D elastic and electric variables. In this work, the prescribed potential in active material is expressed through a set of independent (and given) electric modes and their dimensionless amplitudes. The induced potential in active material is obtained from a constrained minimization problem over the cross section.

There are another significant body of literature on beam models based on the celebrated Saint–Venant principle (Giavotto et al., 1983; Dong et al., 2001). The 3D displacements are represented using a Ritz-type approximation in terms of six rigid body motions (three translations and three rotations) of the cross section, which are only functions of the beam axis, and warping functions which strain the cross section. Then variational principles such as the principle of virtual work or the principle of minimum total potential energy can be used to derive a set of ordinary differential equations in terms of the beam axis and the coefficients are unknown functions of the two cross-sectional coordinates. The advantage of this method is that both ''central'' solution (the beam problem) and ''extremity'' solution (end effects) can be analyzed within the same framework, although it is not trivial to extend this method to geometrically nonlinear analysis. This method has also been generalized to deal with beams made of smart materials (Ghiringhelli et al., 1997; Taciroglu et al., 2004).

In this paper, we start from the original, geometrically nonlinear, 3D formulation of the active structure and rigorously decouple it into a two-dimensional (2D) coupled cross-sectional analysis and a 1D geometrically nonlinear beam analysis. No assumptions have been made on the distribution of mechanical and

electric field inside structure. The prescribed potential are represented accurately using point constraints. The dielectric properties of both active materials and passive materials have been taken into consideration. No assumption has been made on the induced potential distribution over the cross section, rather it is solved as an unknown inside the active as well as the passive material. Also compared to the Ritz-type procedure in Palacios and Cesnik (2005), the present formulation is a direct extension of the Variational Asymptotic Beam Sectional Analysis (Yu, 2002) to electromechanical systems, which is much simpler and more tractable.

2. Three-dimensional formulation

The elastodynamic behavior of any structure is governed by the Hamilton's principle

$$\int_{t_1}^{t_2} [\delta(\mathcal{K} - \mathcal{U}) + \overline{\delta \mathcal{W}}]\, \mathrm{d}t = 0 \tag{1}$$

where t_1 and t_2 are arbitrary fixed times, $\mathcal{K}$ is the kinetic energy, $\mathcal{U}$ is an energy term related the internal energy, and $\overline{\delta \mathcal{W}}$ is the virtual work of applied loads and electric charges (if exist). The bar is used to indicate that the virtual work needs not be the variations of functionals. An active beam is a structure made of active materials, which implies that the internal energy will be characterized by the mechanical field and one or more other fields. For piezoelectrics, $\mathcal{U}$ is the so-called electric enthalpy, which is the Legendre transformation of the internal energy (Le, 1999)

$$\mathcal{U} = \frac{1}{2} \int_{\mathcal{V}} (\boldsymbol{\Gamma}^{\boldsymbol{T}} : \boldsymbol{C}^{\boldsymbol{E}} : \boldsymbol{\Gamma} - 2\boldsymbol{E} \cdot \boldsymbol{e} : \boldsymbol{\Gamma} - \boldsymbol{E}^{\boldsymbol{T}} \cdot \boldsymbol{\varepsilon}^{\boldsymbol{\Gamma}} \cdot \boldsymbol{E})\, \mathrm{d}\mathcal{V} \tag{2}$$

where $\boldsymbol{C}^{\boldsymbol{E}}$ is the elastic tensor at constant electric field, $\boldsymbol{\Gamma}$ is the strain tensor, $\boldsymbol{e}$ is the piezoelectric tensor, $\boldsymbol{E}$ is the electric field vector, $\boldsymbol{\varepsilon}^{\boldsymbol{\Gamma}}$ is the dielectric tensor at constant strain field, and $\mathcal{V}$ is the space occupied by the structure. It is noted that although we use smart structures made of piezoelectrics, the present formulation is equally applicable to smart structures made of other smart materials characterized by a constitutive model with the same mathematical structure as Eq. (2).

As sketched in Fig. 1, a beam can be represented by a reference line r measured by x_1, and a typical cross section Ω with h as its characteristic dimension and described by cross-sectional Cartesian coordinates x_α.

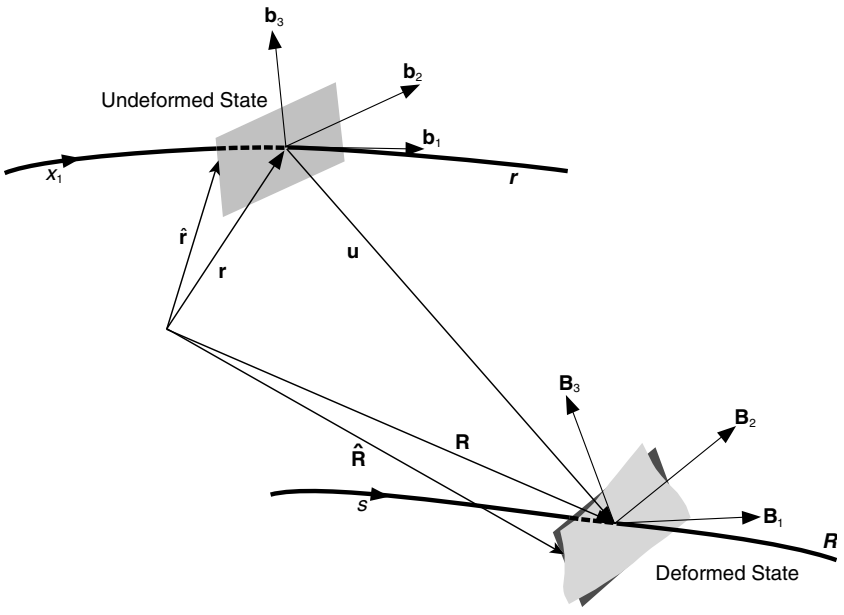

Fig. 1. Schematic of beam deformation.

(Here and throughout the paper, Greek indices assume values 2 and 3 while Latin indices assume 1, 2, and 3. Repeated indices are summed over their range except where explicitly indicated.) At each point along r, an orthonormal triad $\mathbf{b}_i$ is introduced such that $\mathbf{b}_i$ is tangent to x_i. Any point of the undeformed structure is located by the position vector $\widehat{\mathbf{r}}$ as

$$\widehat{\mathbf{r}}(x_1,x_2,x_3) = \mathbf{r}(x_1) + x_\alpha \mathbf{b}_\alpha \tag{3}$$

where $\mathbf{r}$ is the position vector of the points of the reference line, $\mathbf{r}' = \mathbf{b}_1$ with $()' = \frac{\partial()}{\partial x_1}$. After deformation, the particle that had position vector $\widehat{\mathbf{r}}$ in the undeformed state now has the position vector $\widehat{\mathbf{R}}$ in the deformed state, such that

$$\widehat{\mathbf{R}}(x_1,x_2,x_3) = \mathbf{R}(x_1) + x_\alpha \mathbf{B}_\alpha(x_1) + w_i(x_1,x_2,x_3)\mathbf{B}_i(x_1) \tag{4}$$

where $\mathbf{R}$ is the position vector of the reference line for the deformed structure, $\mathbf{B}_i$ forms an orthonormal triad for the deformed configuration so that $\mathbf{B}_1$ is tangent to the deformed reference line, and w_i are the warping functions, which are introduced to accommodate all possible deformation other than those described by $\mathbf{R}$ and $\mathbf{B}_i$.

Using the concept of decomposition of rotation tensor (Danielson and Hodges, 1987), we can express the Jaumann–Biot–Cauchy strains valid for small local rotation as

$$\Gamma_{ij} = \frac{1}{2}(F_{ij} + F_{ji}) - \delta_{ij} \tag{5}$$

where δ_{ij} is the Kronecker symbol, and F_{ij} the mixed-basis component of the deformation gradient tensor such that

$$F_{ij} = \mathbf{B}_i \cdot \mathbf{G}_k \mathbf{g}^k \cdot \mathbf{b}_j \tag{6}$$

with $\mathbf{G}_k$ as the covariant base vectors of the deformed configuration and $\mathbf{g}^k$ as the contravariant base vectors of the undeformed configuration. The 1D generalized strain measures can be defined in the following intrinsic form:

$$\begin{aligned} \gamma_{11}\mathbf{b}_1 &= \mathbf{b}_i\mathbf{B}_i \cdot \mathbf{R}' - \mathbf{r}' \\ \kappa_i \mathbf{b}_i &= \mathbf{b}_i\mathbf{B}_i \cdot \mathbf{K} - \mathbf{k} \end{aligned} \tag{7}$$

where $\mathbf{K}$ is the curvature vector of the deformed reference line, $\mathbf{k}$ is the curvature vector of the undeformed reference line, γ_{11} is the extensional strain, κ_1 is the twist, and κ_α are the bending curvatures. Using Eq. (5) along with Eqs. (6), (7), (3), and (4), we can express the 3D strain field, Γ_{ij}, in terms of 1D generalized strains (γ_{11} and κ_i) and the warping functions, w_i. Up to this point, we have obtained an exact formulation for the kinematics of the mechanical field of smart beams, which is the same as conventional composite beams in Yu et al. (2002).

However, a complete description of smart beams requires not only the mechanical field but also the electric field, which is characterized by the electric potential, $\phi(x_i)$, as

$$\mathbf{E} = -\nabla\phi = -\frac{\partial\phi}{\partial x_i}\mathbf{g}^i \tag{8}$$

whose components in $\mathbf{b}_i$ system are

$$E_1 = -\frac{\phi' + \left(x_3\frac{\partial\phi}{\partial x_2} - x_2\frac{\partial\phi}{\partial x_3}\right)k_1}{\sqrt{g}}, \quad E_2 = -\frac{\partial\phi}{\partial x_2}, \quad E_3 = -\frac{\partial\phi}{\partial x_3} \tag{9}$$

where k_1 is the initial twist. In the present study, surface mounted or embedded smart materials are coated with electrodes on surfaces parallel to the beam reference line. Electroded surfaces could form equipotential regions with prescribed electric potential. Most of the current applications of smart beams use this kind of electrode arrangement. When the smart beam is electroded, except those locations where the electric potential is applied from outside source, the electric potential distribution is an unknown 3D function.

For the convenience of derivation, we introduce the following matrix notations:

$$\begin{aligned}\epsilon &= \lfloor \gamma_{11}\ \kappa_1\ \kappa_2\ \kappa_3 \rfloor^{\mathrm{T}} \\ \widehat{w} &= \lfloor w_1\ w_2\ w_3\ \phi \rfloor^{\mathrm{T}} \\ \Gamma &= \lfloor \Gamma_{11}\ 2\Gamma_{12}\ 2\Gamma_{13}\ \Gamma_{22}\ 2\Gamma_{23}\ \Gamma_{33}\ E_1\ E_2\ E_3 \rfloor^{\mathrm{T}}\end{aligned} \tag{10}$$

From Eqs. (5) and (9), we have the following

$$\Gamma = \Gamma_h \widehat{w} + \Gamma_\epsilon \epsilon + \Gamma_R \widehat{w} + \Gamma_l \widehat{w}' \tag{11}$$

with the operator matrices are explicitly given as:

$$\Gamma_h = \begin{bmatrix} 0 & 0 & 0 & 0 \\ \frac{\partial}{\partial x_2} & 0 & 0 & 0 \\ \frac{\partial}{\partial x_3} & 0 & 0 & 0 \\ 0 & \frac{\partial}{\partial x_2} & 0 & 0 \\ 0 & \frac{\partial}{\partial x_3} & \frac{\partial}{\partial x_2} & 0 \\ 0 & 0 & \frac{\partial}{\partial x_3} & 0 \\ 0 & 0 & 0 & 0 \\ 0 & 0 & 0 & -\frac{\partial}{\partial x_2} \\ 0 & 0 & 0 & -\frac{\partial}{\partial x_3} \end{bmatrix}, \qquad \Gamma_\epsilon = \frac{1}{\sqrt{g}} \begin{bmatrix} 1 & 0 & x_3 & -x_2 \\ 0 & -x_3 & 0 & 0 \\ 0 & x_2 & 0 & 0 \\ 0 & 0 & 0 & 0 \\ 0 & 0 & 0 & 0 \\ 0 & 0 & 0 & 0 \\ 0 & 0 & 0 & 0 \\ 0 & 0 & 0 & 0 \\ 0 & 0 & 0 & 0 \end{bmatrix}, \tag{12}$$

$$\Gamma_R = \frac{1}{\sqrt{g}} \begin{bmatrix} k^* & -k_3 & k_2 & 0 \\ k_3 & k^* & -k_1 & 0 \\ -k_2 & k_1 & k^* & 0 \\ 0 & 0 & 0 & 0 \\ 0 & 0 & 0 & 0 \\ 0 & 0 & 0 & 0 \\ 0 & 0 & 0 & -k^* \\ 0 & 0 & 0 & 0 \\ 0 & 0 & 0 & 0 \end{bmatrix}, \qquad \Gamma_l = \frac{1}{\sqrt{g}} \begin{bmatrix} 1 & 0 & 0 & 0 \\ 0 & 1 & 0 & 0 \\ 0 & 0 & 1 & 0 \\ 0 & 0 & 0 & 0 \\ 0 & 0 & 0 & 0 \\ 0 & 0 & 0 & 0 \\ 0 & 0 & 0 & -1 \\ 0 & 0 & 0 & 0 \\ 0 & 0 & 0 & 0 \end{bmatrix} \tag{13}$$

where $k^* = k_1(x_3 \frac{\partial}{\partial x_2} - x_2 \frac{\partial}{\partial x_3})$, $\sqrt{g} = 1 - x_2 k_3 + x_3 k_2$, and k_α are the initial curvatures. The electric enthalpy can be easily calculated by substituting Eq. (11) into Eq. (2) as

$$\mathcal{U} = \frac{1}{2} \int_0^L \left\langle \Gamma^{\mathrm{T}} \begin{bmatrix} C^E & -e^{\mathrm{T}} \\ -e & -\varepsilon^\Gamma \end{bmatrix} \Gamma \sqrt{g} \right\rangle \mathrm{d}x_1 \equiv \frac{1}{2} \int_0^L \langle \Gamma^{\mathrm{T}} C \Gamma \sqrt{g} \rangle \, \mathrm{d}x_1 \tag{14}$$

where L denotes the length of the beam, the angle brackets signify integration of the argument over the cross-sectional plane, and C^E, e, ε^Γ are matrices formed by the components of corresponding tensors $\boldsymbol{C}^{\boldsymbol{E}}$, $\boldsymbol{e}$, $\boldsymbol{\varepsilon}^{\boldsymbol{\Gamma}}$, respectively. For regular composite material which is not piezoelectric, the piezoelectric matrix e is zero but the dielectric matrix ε^Γ is in general not zero.

To calculate the kinetic energy, we need to know the absolute velocity of a generic point in the structure by taking a time derivative of Eq. (4), such that

$$v = V + \widetilde{\Omega}(\xi + w) + \dot{w} \tag{15}$$

where $\dot{()}$ is the partial derivative with respect to time, V is the absolute velocity of a point in the deformed reference line, Ω is the inertial angular velocity of $\mathbf{B}_i$ bases, and the notation $\widetilde{()}$ forms an antisymmetric matrix from a vector according to $\widetilde{()}_{ij} = -e_{ijk}()_k$ using the permutation symbol e_{ijk}. In Eq. (15), the symbols v, V, Ω, w denote column matrices containing the components of corresponding vectors in $\mathbf{B}_i$ bases, and $\xi = \lfloor 0\, x_2\ x_3 \rfloor^{\mathrm{T}}$. The kinetic energy of a beam can be obtained by

$$\mathcal{K} = \frac{1}{2}\int_{\mathcal{V}} \rho v^{\mathrm{T}} v \,\mathrm{d}\mathcal{V} = \mathcal{K}_{1\mathrm{D}} + \mathcal{K}^{*} \tag{16}$$

where ρ is the mass density and

$$\mathcal{K}_{1\mathrm{D}} = \frac{1}{2}\int_0^L (\eta V^T V + 2\Omega^{\mathrm{T}}\widetilde{\eta\bar{\xi}}V + \Omega^{\mathrm{T}} i\Omega)\,\mathrm{d}x_1 \tag{17}$$

$$\mathcal{K}^{*} = \frac{1}{2}\int_{\mathcal{V}} \rho[(\widetilde{\Omega}w + \dot{w})^{\mathrm{T}}(\widetilde{\Omega}w + \dot{w}) + 2(V + \widetilde{\Omega}\xi)^{\mathrm{T}}(\widetilde{\Omega}w + \dot{w})]\,\mathrm{d}\mathcal{V} \tag{18}$$

with $\eta, \eta\bar{\xi}$, and i defined as mass per unit length, the first and second distributed mass moments of inertia, respectively, which can be trivially obtained through simple integrals over the cross-section (Hodges, 2006).

If no electric charges applied on the surfaces or inside the body, the virtual work of the active beam is completely done by applied loads and can be calculated as

$$\overline{\delta\mathcal{W}} = \int_0^L \left(\langle \mathbf{F}\cdot\delta\widehat{\mathbf{R}}\sqrt{g}\rangle + \oint_{\partial\Omega}\mathbf{Q}\cdot\delta\widehat{\mathbf{R}}\,\mathrm{d}s\right)\mathrm{d}x_1 + \langle \mathbf{Q}\cdot\delta\widehat{\mathbf{R}}\rangle|_{x_1=0}^{x_1=L} \tag{19}$$

where $\partial\Omega$ denotes the lateral surface of the beam, $\mathbf{F} = F_i\mathbf{B}_i$ is the applied body force, $\mathbf{Q} = Q_i\mathbf{B}_i$ is the applied surface tractions. $\delta\widehat{\mathbf{R}}$ is the Lagrangian variation of the displacement field, such that

$$\delta\widehat{\mathbf{R}} = \overline{\delta q}_i\mathbf{B}_i + x_\alpha\delta\mathbf{B}_\alpha + \delta w_i\mathbf{B}_i + w_j\delta\mathbf{B}_j \tag{20}$$

where the virtual displacement and rotation are defined as

$$\overline{\delta q}_i = \delta\mathbf{R}\cdot\mathbf{B}_i \qquad \delta\mathbf{B}_i = \overline{\delta\psi}_j\mathbf{B}_j\times\mathbf{B}_i \tag{21}$$

where $\overline{\delta q}_i$ and $\overline{\delta\psi}$ contain the components of the virtual displacement and rotation in the $\mathbf{B}_i$ system, respectively. Since the warping functions are small, one may safely ignore products of the warping and virtual rotation in $\delta\widehat{\mathbf{R}}$ and obtain the virtual work due to applied loads as

$$\overline{\delta\mathcal{W}} = \overline{\delta\mathcal{W}}_{1\mathrm{D}} + \overline{\delta\mathcal{W}}^{*} \tag{22}$$

where

$$\overline{\delta\mathcal{W}}_{1\mathrm{D}} = \int_0^L (f_i\overline{\delta q}_i + m_i\overline{\delta\psi}_i)\,\mathrm{d}x_1 + \langle Q_i\rangle\overline{\delta q}_i|_{x_1=0}^{x_1=L} + e_{i\alpha j}\langle x_\alpha Q_j\rangle\overline{\delta\psi}_i|_{x_1=0}^{x_1=L} \tag{23}$$

$$\overline{\delta\mathcal{W}}^{*} = \int_0^L \left(\langle F_i\sqrt{g}\delta w_i\rangle + \oint Q_i\delta w_i\,\mathrm{d}s\right)\mathrm{d}x_1 + \langle Q_i\delta w_i\rangle|_{x_1=0}^{x_1=L} \tag{24}$$

with the generalized forces f_i and moments m_i defined as

$$f_i = \langle F_i\sqrt{g}\rangle + \oint Q_i\,\mathrm{d}s \qquad m_i = e_{i\alpha j}\left(\langle x_\alpha F_j\sqrt{g}\rangle + \oint x_\alpha Q_j\,\mathrm{d}s\right) \tag{25}$$

Then the Hamilton's principle in Eq. (1) becomes

$$\int_{t_1}^{t_2}\left[\delta(\mathcal{K}_{1\mathrm{D}} + \mathcal{K}^{*} - \mathcal{U}) + \overline{\delta\mathcal{W}}_{1\mathrm{D}} + \overline{\delta\mathcal{W}}^{*}\right]\mathrm{d}t = 0 \tag{26}$$

So far, we have presented a 3D formulation for the electromechanically coupled problem of smart beams in terms of 1D displacements (represented by $\mathbf{R} - r$) and rotations (represented by $\mathbf{b}_i\mathbf{B}_i$) and 3D warping functions (w_i and ϕ). Hereafter, we use warping functions to indicate both the 3D mechanical warping functions w_i and the electric potential ϕ except where explicitly indicated. If we attempt to solve this problem directly, we will meet the same difficulty as solving any full 3D problem. The main complexity comes from the unknown 3D warping functions w_i and ϕ. The common practice in the literature is to assume w_i, a priori, in terms of 1D displacements and rotations, and ϕ in terms of applied electric potential to straightforwardly reduce the original 3D continuum model into a 1D beam model. However, for beams made with generally composite materials, the imposition of such a priori assumptions may introduce significant errors. The accuracy of the

reduced beam model becomes worse when there exist multiple fields in the structure. Fortunately, VAM provides a powerful technique to obtain w_i and ϕ through an asymptotical analysis of the variational statement in Eq. (26) in terms of small parameters inherent in the structure to construct asymptotically correct 1D beam models. The rest of the paper will show how this could be accomplished for smart slender structures.

3. Dimensional reduction

The dimensional reduction from the original 3D formulation to a 1D formulation can only be done approximately. The best way to do it is to take advantage of the small parameters in the formulation to construct the 1D formulation so that an asymptotically correct approximation to the original 3D formulation can be achieved.

3.1. Asymptotical analysis

For a structure to be modeled as a beam, it should be slender, which means $h/l \ll 1$ and $h/R \ll 1$, with h as the characteristic size of the cross-section, l the characteristic wavelength of axial deformation and R the characteristic radius of initial curvatures and twist of the beam. For simplicity, we assume R and l are of similar order, which means $\bar{h} \sim h/l \sim h/R \ll 1$.

The strain is also small if we are only interested in a geometrically nonlinear but physically linear 1D theory, i.e., $\bar{\epsilon} \ll 1$. Here, $\bar{\epsilon}$ denotes the characteristic magnitude of ϵ. From the 1D equations of motion (Hodges, 2006), we can estimate the following orders of the applied forces and moments:

$$F_1 \sim \mathrm{O}(\mu\bar{h}\bar{\epsilon}/h), \quad Q_1 \sim \mathrm{O}(\mu\bar{h}\bar{\epsilon}), \quad F_\alpha \sim \mathrm{O}(\mu\bar{h}^2\bar{\epsilon}/h), \quad Q_\alpha \sim \mathrm{O}(\mu\bar{h}^2\bar{\epsilon}) \tag{27}$$

with μ denoting the order of the elastic constants. For low-frequency vibrations, we also have the following small parameter

$$\frac{h}{c_s\tau} \sim \mathrm{O}(\bar{h}) \ll 1 \tag{28}$$

where τ is the characteristic scale of change of the displacement and warping functions in time and $c_s = \sqrt{\mu/\rho}$, the characteristic velocity of shear waves.

According to VAM, and in view of the order assessments in Eqs. (27) and (28), we can obtain the leading terms of the variational statement in Eq. (26) as

$$\int_{t_1}^{t_2} \left[\delta(\mathcal{K}_{1D} - \int_0^L \mathcal{H}_0 \mathrm{d}x_1) + \overline{\delta\mathcal{W}}_{1D}\right] \mathrm{d}t = 0 \tag{29}$$

where $\mathcal{H}_0$ denotes the zeroth-order internal energy per unit span, such that

$$\mathcal{H}_0 = \frac{1}{2}\langle \Gamma_0^{\mathrm{T}} C \Gamma_0 \rangle \tag{30}$$

with

$$\Gamma_0 = \Gamma_h \widehat{w} + \Gamma_\epsilon \epsilon \tag{31}$$

It is clear that the unknown 3D warping function w_i and ϕ only appear in $\mathcal{H}_0$, which means w_i and ϕ can be solved from the following much simpler variational statement:

$$\delta\mathcal{H}_0 = 0 \tag{32}$$

3.2. Solution of the warping functions

It can easily be checked that the warping field $\hat{w}$ over the cross section follows a mathematical structure of an *inner product space*, $(V_{\Omega(x_1)}, \langle *, * \rangle)$, where $V_{\Omega(x_1)} = \{\widehat{w}(x_1, x_2, x_3) | (x_2, x_3) \in \Omega(x_1), x_1 \in [0, l]\}$. From Eq. (31), it is clear that if warping has to contribute to the zeroth-order energy, then it should not satisfy the equation

$\Gamma_h\hat{w} = 0$; in other words admissible solution of warping field should be orthogonal to the null space of the operator Γ_h, which can easily be found by solving the differential equations coming from $\Gamma_h\hat{w} = 0$ as:

$$\begin{aligned} w_1 &= c_1 \\ w_2 &= c_2 - c_4 x_3 \\ w_3 &= c_3 + c_4 x_2 \\ \phi &= c_5 \end{aligned} \tag{33}$$

Successively making each constant $c_i = 1$ and all other zero, one at a time, one can easily get five vectors which span the null space given as:

$$\psi_1 = \begin{bmatrix} v_1 & v_2 & v_3 & v_4 & v_5 \\ 1 & 0 & 0 & 0 & 0 \\ 0 & 1 & 0 & -x_3 & 0 \\ 0 & 0 & 1 & x_2 & 0 \\ 0 & 0 & 0 & 0 & 1 \end{bmatrix} \tag{34}$$

The solutions of unknown warping functions, $\widehat{w} \in \psi_1^{\perp}$ and mathematically given as

$$\langle \widehat{w}^{\mathrm{T}} \psi_1 \rangle = 0 \tag{35}$$

Eq. (35) reduces down to five scalar equations, the first four of which are the same as the constraints on mechanical warping given in Yu et al. (2002) and the last equation boils down to $c_5\langle\phi\rangle = 0$. However, due to the existence of the externally applied potential over the cross section, $\langle\phi\rangle \neq 0$ in general, which implies $c_5 = 0$. Hence, the dimension of the null space turns out to be four and spanned by v_1, v_2, v_3, and v_4. Now, the four integral constraints on the warping field can be written as:

$$\langle \widehat{w}^{\mathrm{T}} \psi \rangle = 0 \tag{36}$$

where $\psi = [v_1\ v_2\ v_3\ v_4]$.

In order to deal with arbitrary cross-sectional geometry and general anisotropic materials, we need to rely on a numerical approach, such as the finite element method (FEM), to find the warping functions. The warping field can be discretized as

$$\widehat{w}(x_1, x_2, x_3) = S(x_2, x_3)V(x_1) \tag{37}$$

with $S(x_2, x_3)$ representing the element shape functions and V as a column matrix of the nodal values of the warping functions over the cross section. Substituting Eq. (37) into Eq. (31) and then into Eq. (30), we obtain

$$2\mathcal{U}_0 = V^{\mathrm{T}} E V + 2V^{\mathrm{T}} D_{h\epsilon}\epsilon + \epsilon^{\mathrm{T}} D_{\epsilon\epsilon}\epsilon \tag{38}$$

with

$$E = \langle [\Gamma_h S]^T C [\Gamma_h S] \rangle, \quad D_{h\epsilon} = \langle [\Gamma_h S]^T C [\Gamma_\epsilon] \rangle, \quad D_{\epsilon\epsilon} = \langle [\Gamma_\epsilon]^T C [\Gamma_\epsilon] \rangle \tag{39}$$

If we discretize ψ such that $\psi = S\Psi$, then constraints in Eq. (36) can also be written in a discretized form as

$$V^{\mathrm{T}} H \Psi = 0 \tag{40}$$

where $H = \langle S^{\mathrm{T}} S \rangle$ and Ψ can be normalized so that $\Psi^{\mathrm{T}} H \Psi = I$ with I as an identity matrix. It is also trivial to verify that $E\Psi = 0$, because Ψ is a subset of the kernel matrix of E.

To deal with applied electric potential in some specific locations, we divide the total nodal values of the warping field into two parts such that

$$V = V_k + V_u \tag{41}$$

where V_k is a known matrix holding the prescribed electric potential at specific points (nodes), and V_u is an unknown matrix such that the electric potential of those prescribed points (nodes) are zeroes. Substituting Eq. (41) into Eq. (38), we rewrite the zeroth-order energy as

$$2\mathcal{H}_0 = V_u^{\mathrm{T}} E V_u + 2V_u^{\mathrm{T}} E V_k + 2V_u^{\mathrm{T}} D_{h\epsilon}\epsilon + 2V_k^T D_{h\epsilon}\epsilon + \epsilon^{\mathrm{T}} D_{\epsilon\epsilon}\epsilon \tag{42}$$

Here the quadratic terms with known potential $V_k^T E V_k$ is dropped because it will not affect our solution. It is noted that V_u are fixed to be zero only for the electric degree of freedom where the electric potential is prescribed, while the constraints in Eq. (40) are applied only to mechanical degrees of freedom, i.e.,

$$V_u^{\mathrm{T}} H \Psi = 0 \tag{43}$$

Since these two types of constraints are completely independent of each other, we can follow the same approach of introducing prescribed displacements in the conventional displacement-based FEM to incorporate zeros at specific nodes for V_u, and use Lagrange multiplier method to introduce the constraints in Eq. (43). The Euler–Lagrange equation for the variational statement in Eq. (32) turns out to be

$$E(V_u + V_k) + D_{h\epsilon}\epsilon = H\Psi\Lambda \tag{44}$$

where Λ contains the Lagrange multipliers enforcing the constraints in Eq. (43). Multiplying both sides by Ψ^{T}, one can obtain:

$$\Lambda = \Psi^{\mathrm{T}} D_{h\epsilon}\epsilon \tag{45}$$

Substituting Eq. (45) into Eq. (44), we get

$$E V_u = (H\Psi\Psi^{\mathrm{T}} - I) D_{h\epsilon}\epsilon - E V_k \tag{46}$$

As pointed out in Yu (2002), there exists a unique solution linearly independent of Ψ for V_u because the right hand side of Eq. (46) is orthogonal to Ψ, the null space of E. The final solution of Eq. (46) can be written symbolically as

$$V_u = V_0\epsilon + V_\phi \tag{47}$$

Substituting Eq. (47) into Eq. (42) and using the following identity derived from Eq. (44)

$$V_u^{\mathrm{T}} E V_u + V_u^{\mathrm{T}} E V_k + V_u^{\mathrm{T}} D_{h\epsilon}\epsilon = 0 \tag{48}$$

we obtain the zeroth-order approximation of the electric enthalpy as

$$2\mathcal{H}_0 = \epsilon^{\mathrm{T}}(\widehat{V}_0^{\mathrm{T}} D_{h\epsilon} + D_{\epsilon\epsilon})\epsilon + \epsilon^{\mathrm{T}}(\widehat{V}_0 E V_k + D_{h\epsilon}^{\mathrm{T}} V_\phi + 2D_{h\epsilon}^{\mathrm{T}} V_k) \tag{49}$$

Here a term which is not related with ϵ, $V_\phi^T E V_k$, is dropped because it will not affect our beam model. Now, we have managed to solve the unknown warping functions w_i and ϕ in terms of 1D generalized strains and known electric potential prescribed on the cross section. With the knowledge of $\mathcal{U}_0$ in Eq. (49), the variational statement in Eq. (29) becomes a 1D formulation suitable for a geometrically nonlinear beam analysis.

If we define the 1D generalized sectional resultants conjugate to ϵ, such that

$$F = \frac{\partial \mathcal{H}_0}{\partial \epsilon} \tag{50}$$

then we can obtain a 1D constitutive model for the classical beam analysis of smart beams as

$$\begin{bmatrix} F_1 \\ M_1 \\ M_2 \\ M_3 \end{bmatrix} = S\epsilon - f^a = \begin{bmatrix} s_{11} & s_{12} & s_{13} & s_{14} \\ s_{12} & s_{22} & s_{23} & s_{24} \\ s_{13} & s_{23} & s_{33} & s_{34} \\ s_{14} & s_{24} & s_{34} & s_{44} \end{bmatrix} \begin{bmatrix} \gamma_{11} \\ \kappa_1 \\ \kappa_2 \\ \kappa_3 \end{bmatrix} - \begin{bmatrix} f_1^a \\ m_1^a \\ m_2^a \\ m_3^a \end{bmatrix} \tag{51}$$

with the stiffness matrix S obtained as

$$S = \widehat{V}_0^{\mathrm{T}} D_{h\epsilon} + D_{\epsilon\epsilon} \tag{52}$$

and the actuation force vector $f^{(a)}$ obtained as

$$f^a = -\frac{1}{2}\left(\widehat{V}_0 E V_k + D_{h\epsilon}^{\mathrm{T}} V_\phi + 2D_{h\epsilon}^{\mathrm{T}} V_k\right) \tag{53}$$

From Eq. (51), it is clear that the electric potential is not a variable in the 1D problem, which implies that we can not get a coupled actuator–sensor equation directly in the beam model itself. Nevertheless, we can solve the 1D problem for the 1D strains ϵ and we can compute the 3D strains and electric potential from Eqs. (47), (41), and (31). Finally, we can also obtain the charge densities from 3D constitutive relations in Eq. (2) for sensing purpose.

4. Model verification

The above developed theory for dimensional reduction of smart beams has been implemented into the computer program VABS. To demonstrate the application of this theory and verify the veracity of the model, we have used VABS to carry out the cross-sectional analysis of several smart beams and compared results with those available in the literature and 3D multiphysics simulation in ANSYS.

The present theory completely decouples the cross-sectional analysis from the global beam analysis, which means we only need to carry out the cross-sectional analysis once to compute the cross-sectional constants and these constants can be used as inputs for various beam analyses. Since the focus of the present work is the cross-sectional analysis, we need to verify the accuracy of cross-sectional constants obtained by the cross-sectional analysis. To this end, UM/VABS (Palacios and Cesnik, 2005), a general-purpose cross-sectional analysis code capable of modeling smart beam sections, is the most direct and appropriate tool for validating the present theory and the companion code VABS. Besides UM/VABS, most smart beam models in the literature (Robbins and Reddy, 1991; Saravanos and Heyliger, 1995) do not separate the cross-sectional analysis and the global beam analysis, for us to compare with these approaches, we need to input the cross-sectional constants into a 1D beam analysis, such as the geometrically exact beam theory in Han et al. (2007), to calculate the global behavior for comparison. Of course, the ultimate validation of the present theory will be a 3D finite element analysis capable of dealing with piezoelectric materials, such as the multiphysics simulation of ANSYS.

4.1. Three-layer smart beam

A three-layer rectangular beam composed of a piezoelectric layer, an adhesive layer, and a composite T300/934 base layer has been extensively studied in Saravanos and Heyliger (1995) by introducing kinematic assumptions for each layer (a layerwise theory). The details of the construction are given in Saravanos and Heyliger (1995) and the material and geometry properties are listed in Table 1. A voltage of 12.49 kV is applied to the top of piezoelectric layer and the bottom of the piezoelectric layer is grounded.

We mesh this cross section with 100 8-noded quadrilateral elements (10 elements along the width, six elements along the thickness of the T300/934 layer, two elements along the thickness of the adhesive layer and the piezoelectric layer). The cross-sectional constants calculated by VABS are listed in Table 2 along with the

Table 1
Geometry and material properties of the three-layer smart beam

Properties	T300/934	Adhesive	Piezoelectric
$E_{11} = E_{33}$ (GPa)	126.0	6.9	68.9
E_{33} (GPa)	7.9	6.9	48.3
ν_{13}	0.275	0.4	0.25
$G_{12} = G_{13} = G_{23}$ (GPa)	27.6	2.46	31
$e_{31} = e_{32}$ $(\frac{C}{m^2})$	0	0	−7.99
$e_{33}(\frac{C}{m^2})$	0	0	14.86
$e_{24} = e_{15}$ $(\frac{C}{m^2})$	0	0	15.37
ε^S_{11} $(\frac{C}{Vm})$	3.09×10^{-11}	5.43×10^{-9}	5.43×10^{-9}
ε^S_{22} $(\frac{C}{Vm})$	2.65×10^{-11}	5.43×10^{-9}	5.43×10^{-9}
ε^S_{33} $(\frac{C}{Vm})$	2.65×10^{-11}	5.32×10^{-9}	5.32×10^{-9}
Thickness (mm)	15.24	0.254	1.524
Width (mm)	25.4	25.4	25.4

Table 2
Cross-sectional constants of the three-layer smart beam

	VABS	UM/VABS^T	Diff. (%)	UM/VABS^C	Diff. (%)
s_{11} (N)	0.5203343×10^8	0.5203342×10^8	0.000	0.5203343×10^8	0.000
s_{13} (N m)	-0.1815134×10^5	-0.1815054×10^4	−0.004	-0.1815054×10^4	0.000
s_{22} (N m^2)	0.1312092×10^3	0.1312093×10^3	0.000	0.1312093×10^3	0.000
s_{33} (N m^2)	0.1178293×10^4	0.1178205×10^3	−0.005	0.1178294×10^3	0.000
s_{44} (N m^2)	0.2797451×10^4	0.2797451×10^4	0.000	0.2797452×10^4	0.000
f_1^a (N)	0.3257824×10^4	0.3257387×10^4	0.013	0.3257387×10^4	0.000
m_2^a (N m)	0.2520117×10^2	0.2520119×10^2	0.000	0.2520119×10^2	0.000

results computed by UM/VABS using the same mesh. Only nonzero values are tabulated for saving space. The % difference is calculated as (VABS − UM/VABS)/|VABS| × 100. UM/VABS can provide a uncoupled analysis, or so-called temperature analogy (Cesnik and Ortega-Morales, 2001; Cesnik and Palacios, 2003) and a coupled analysis (Palacios and Cesnik, 2005). In Table 2, UM/VABS^T denotes the results of the uncoupled analysis by assuming a priori a linear distribution of the electric potential within the piezoelectric layer, while UM/VABS^C denotes the results of the coupled analysis without such a priori assumptions. It can be observed that VABS agrees with both approaches of UM/VABS very well for this case within difference less than 0.3%. We also observed that the coupled analysis results are very close to uncoupled analysis results which can be explained by three features of this example: (1) the piezoelectric layer is very thin and the real distribution of the potential field is almost linear as shown in Fig. 3; (2) the dielectric coefficients are very small and they will not have significant effects on the cross-sectional constants through a coupled approach; (3) only a very small fraction of the cross section is made of piezoelectrics and the main contributions of the cross-sectional stiffness are from the passive materials.

To check the accuracy of the present model against 3D FEM, we construct a slender smart structure of a length 0.1524 m uniformly spanned by the three-layer rectangular cross section. The length is discretized into 100 divisions. SOLID5 coupled elements are used to carry out a linear analysis in ANSYS. VABS cross-sectional constants are fed into a linear 1D beam analysis and a subsequent 3D recovery is carried out. Fig. 2 plots the transverse deflection of the beam reference line (the locus of the geometric center). It seems the simple beam analysis based on cross-sectional constants calculated by VABS can almost reproduce the global behavior predicted by a full-blown 3D finite element analysis. Fig. 3 is the voltage distribution along the thickness of

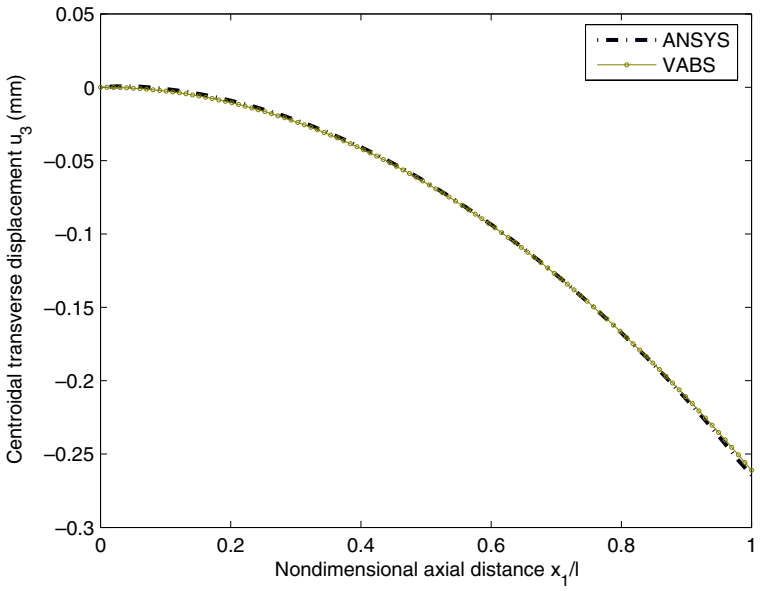

Fig. 2. Transverse displacement.

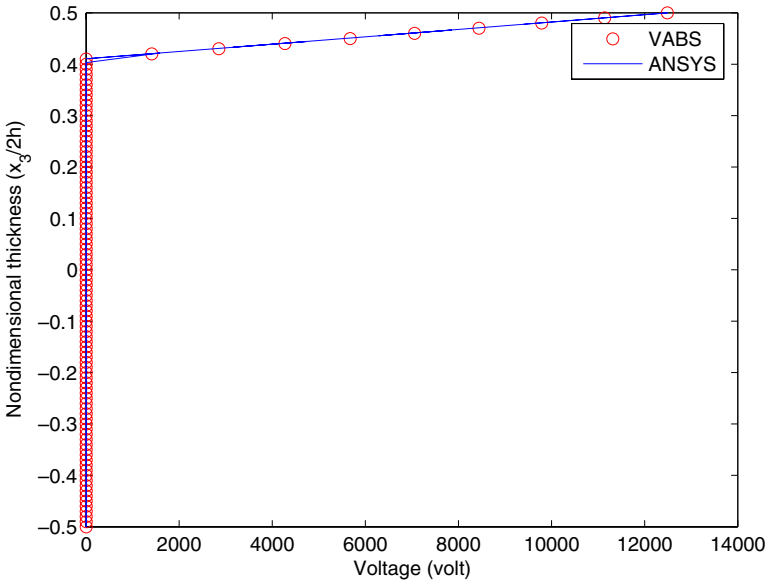

Fig. 3. Voltage variation along the thickness.

the beam, which remains the same along the axis of the beam. Again, the simple beam analysis using VABS has an excellent agreement with the 3D multiphysics simulation of ANSYS. Fig. 4 is the 3D axial displacement variation along the thickness (at $x_2 = 0$, $-0.008509\ \text{m} < x_3 < 0.008509\ \text{m}$) of the beam at the tip location ($x_1 = l$). As the present analysis is a simple classical model, it is seen that the actual through-the-thickness variation predicted by ANSYS is slightly different from those results predicted by VABS near the free end. This may be due to the 3D end effects at the free end boundary which cannot be accurately captured by simple beam models. However, in the interior portion (say $x_1 = 0.5l$) of the beam the recovered 3D distribution from VABS has excellent matches with the 3D ANSYS results as shown in Fig. 5 for axial strain distribution.

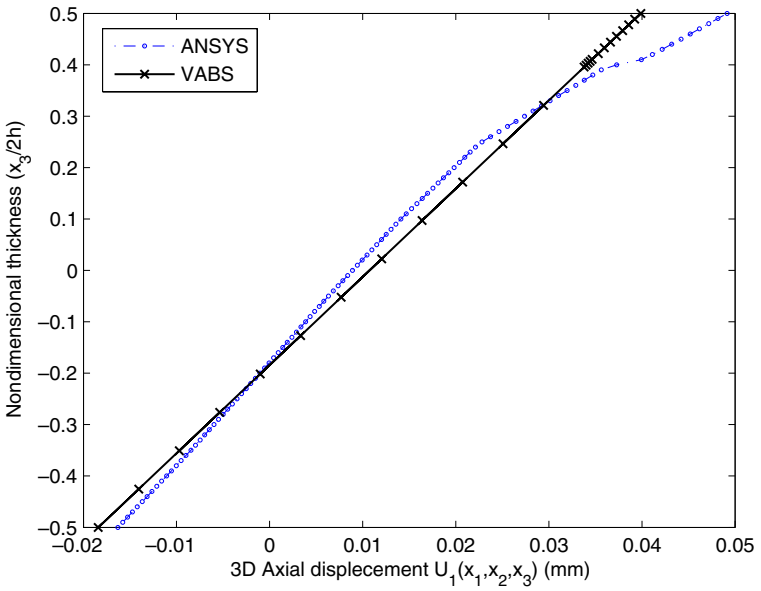

Fig. 4. Axial displacement variation through the thickness at the tip.

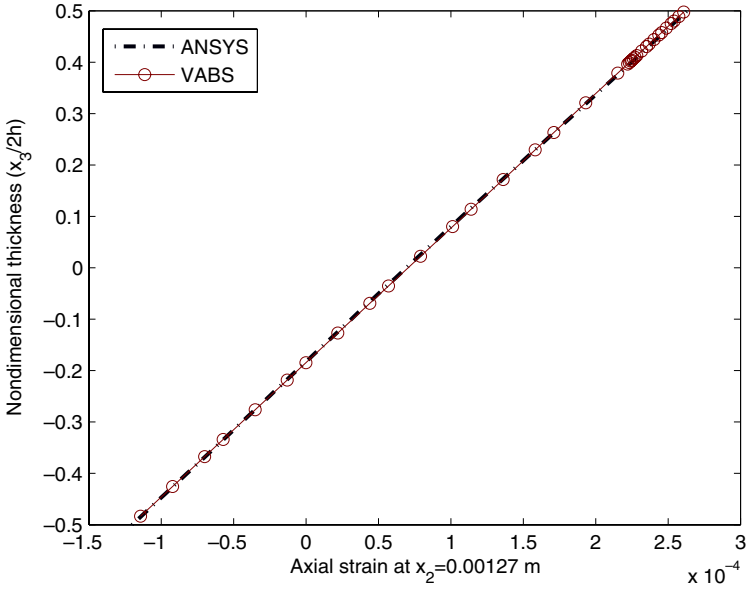

Fig. 5. Axial strain variation at $x_1 = 0.5l$.

4.2. Two-layer smart beam

The second example is a rectangular cross section composed of an aluminum layer bounded to a PZT4 layer. The material and geometry properties are given in Table 3. A voltage of 10 kV is applied on the surface of the PZT4 layer and the interface between the PZT4 layer and the aluminum layer is grounded.

We mesh this cross section with 80 8-noded quadrilateral elements (20 elements along the width, two elements along the thickness of each layer). The cross-sectional constants calculated by VABS are listed in Table 4 along with the results computed by UM/VABS using the same mesh. It can be observed that these three approaches almost predict identical results for extensional stiffness (s_{11}), torsional stiffness (s_{22}), bending stiffness about x_3 direction (s_{44}), and axial actuation force (f_1^a). However, for the bending stiffness about x_2 direction (s_{33}), UM/VABS$^{\mathrm{T}}$ result is slightly smaller than VABS result while UM/VABS$^{\mathrm{C}}$ result is almost the same with VABS result as expected. UM/VABS$^{\mathrm{T}}$ predicts slightly higher values than VABS and UM/VABS$^{\mathrm{C}}$ for the extension-bending stiffness (s_{13}) and actuation bending moment (m_2^a). To assess the accuracy of the different approaches, we create a 3D multiphysics finite element model of a beam of length 200 mm

Table 3
Geometry and material properties of the two-layer smart beam

Properties	Aluminium	PZT4
$E_{11} = E_{22}$ (GPa)	68.9	81.3
E_{33} (GPa)	68.9	64.5
ν_{12}	0.25	0.329
$\nu_{13} = \nu_{23}$	0.25	0.432
G_{12} (GPa)	27.56	30.6
$G_{13} = G_{23}$ (GPa)	27.56	25.6
$e_{31} = e_{32}$ $(\frac{\mathrm{C}}{\mathrm{m}^2})$	0	−5.2
e_{33} $(\frac{\mathrm{C}}{\mathrm{m}^2})$	0	15.08
$e_{24} = e_{15}$ $(\frac{\mathrm{C}}{\mathrm{m}^2})$	0	12.7
$\varepsilon_{11} = \varepsilon_{22}$ $(\frac{\mathrm{C}}{\mathrm{Vm}})$	10.18×10^{-11}	6.761×10^{-9}
ε_{33} $(\frac{\mathrm{C}}{\mathrm{Vm}})$	10.18×10^{-11}	5.874×10^{-9}
Thickness (mm)	5	5
Width (mm)	20	20

Table 4
Cross-sectional constants of the two-layer beam

	VABS	UM/VABS^T	Diff. (%)	UM/VABS^C	Diff. (%)
s_{11} (N)	0.1502593×10^8	0.1502536×10^8	0.0037	0.1502594×10^8	0.000
s_{13} (N m)	0.3062170×10^4	0.3098881×10^4	−1.198	0.3062169×10^4	0.000
s_{22} (N m^2)	0.1300441×10^3	0.1300441×10^3	0.000	0.1300441×10^3	0.000
s_{33} (N m^2)	0.1277671×10^3	0.1252000×10^3	2.00	0.1277672×10^3	0.000
s_{44} (N m^2)	0.5008097×10^3	0.5007985×10^3	0.002	0.5008097×10^3	0.000
f_1^a (N)	0.2024538×10^4	0.2022159×10^4	0.117	0.202454×10^4	0.000
m_2^a (N m)	0.4843378×10^1	0.4995317×10^1	−3.13	0.4843389×10^1	−0.000

made of this two-layer section in ANSYS. Due to the effect of applied electric potential, the structure will be stretched along the axial direction and deflected in the x_3 direction. We also use the geometrically exact active beam analysis developed in Han et al. (2007) to calculate the 1D beam behavior based on the cross-sectional models computed by different approaches. The tip displacements at the center of the cross section computed by different approaches are listed in Table 5 along with ANSYS results which are also obtained by the geometrically nonlinear analysis. The % difference is calculated using (Beam − ANSYS)/|ANSYS| × 100, where Beam could be replaced by VABS, UM/VABS^T, or UM/VABS^C. It can be observed that the axial displacement predictions from different methods are almost the same and UM/VABS^T slightly overpredicts while both VABS and UM/VABS^C slightly underpredicts the deflection result compared to the 3D multiphysics solution.

4.3. Single-layer smart beam

The third example is of a single-layer smart beam completely made of PZT4, which is polarized along the negative x_2 direction. It is a rectangular cross section with thickness (along x_2 direction) equal to 10 mm and width (along x_3 direction) equal to 20 mm. On the x_2 edges, two types of electric boundary conditions are considered: (1) the voltage on $x_2 = 5$ mm was prescribed to be 500 V and the voltage on $x_2 = -5$ mm was prescribed to be −500 V to mimic a closed-circuit (CC) condition; (2) the electric potential is zero on edge $x_2 = 5$ mm and free on edge $x_2 = -5$ mm to simulate an open-circuit (OC) condition. The cross-sectional analysis with CC condition is solved exactly in Le (1999) and the cross-sectional constants can be obtained from closed-form expressions except the torsional stiffness s_{22}. The numerical values obtained from these expressions are listed in Table 6.

We mesh this cross section with 200 8-noded quadrilateral elements (20 elements along the width and ten elements along the thickness of the PZT4 layer). The cross-sectional constants under CC conditions predicted by VABS and UM/VABS are also listed in Table 6. The % difference is calculated with respect to Le (1999).

Table 5
Tip displacements of the two-layer smart beam

Displacement	ANSYS	VABS	Diff. (%)	UM/VABS^T	Diff. (%)	UM/VABS^C	Diff. (%)
u_1 (mm)	−0.0271	−0.0271	*0.00*	−0.0272	0.37	−0.0271	0.00
u_3 (mm)	0.7157	0.6969	−2.63	0.7350	2.70	0.6969	−2.63

Table 6
Closed-circuit cross-sectional constants for the single-layer smart beam

	Le (1999)	VABS	UM/VABS^T	Diff. (%)	UM/VABS^C	Diff. (%)
s_{11} (N)	0.162600×10^8	0.162600×10^8	0.162600×10^8	0.00	0.162600×10^8	0.00
s_{22} (N m^2)	N/A	0.134163×10^3	0.134163×10^3	0.00	0.134163×10^3	0.00
s_{33} (N m^2)	0.542000×10^3	0.542000×10^3	0.542000×10^3	0.00	0.542000×10^3	0.00
s_{44} (N m^2)	0.151722×10^3	0.151722×10^3	0.135500×10^3	10.69	0.151722×10^3	0.00
f_1^a (N)	-0.200075×10^3	-0.200075×10^3	-0.200079×10^3	0.002	-0.200079×10^3	0.002

Table 7
Tip deflection for the closed-circuit case

Displacement	ANSYS	VABS	Diff. (%)	UM/VABS^T	Diff. (%)	UM/VABS^C	Diff. (%)
u_2 (mm)	0.260920	0.263640	1.04	0.295199	13.14	0.263636	1.04

Table 8
Open-circuit cross-sectional constants for the single-layer smart beam

Stiffness	VABS	UM/VABS^C	Diff. (%)
s_{11} (N)	0.182066×10^8	0.182068×10^8	0.000
s_{22} (N m^2)	0.134163×10^3	0.134163×10^3	0.000
s_{33} (N m^2)	0.576249×10^3	0.576253×10^3	0.000
s_{44} (N m^2)	0.151721×10^3	0.151724×10^3	0.000

VABS and UM/VABS^C results are almost identical to the exact solution, while temperature analogy result coming from UM/VABS^T significantly underpredicts the bending stiffness (s_{44}). It is noted that for a real CC condition with electric potentials on $x_2 = \pm 5$ mm surfaces prescribed to be zero, the cross-sectional constants will remain the same except that the axial actuation force vanishes. To verify the validity of the bending stiffness s_{44} predicted by the coupled approach, we again use ANSYS to simulate a cantilever beam of length 200 mm made of this single-layer section. A bending moment $M_3 = 2$ N m is applied at the tip. The tip deflection in x_3 direction is listed in Table 7, which shows that the 1D behavior obtained using the VABS and UM/VABS^C cross-sectional model provides a much better approximation to the result obtained from the coupled 3D analysis using ANSYS than that that from the temperature analogy approach in UM/VABS^T.

No exact solution is available for the OC condition, and UM/VABS^T is not capable to deal with such electric boundary conditions. Hence we only compare the results from VABS along with UM/VABS^C in Table 8 and both of the approaches predict the same result in this case.

5. Conclusion

An asymptotically correct classical beam model has been developed for smart structures via a rigorous dimensional reduction of the original, 3D, geometrically nonlinear, multiphysics formulation of the smart structures. Taking advantage of the slenderness of the structure, we asymptotically split the original 3D problem into a 2D, coupled cross-sectional analysis and a 1D beam analysis. The cross-sectional analysis has been implemented using FEM in the computer program VABS, which can provide an asymptotically correct, 1D constitutive model for smart beams without special assumptions regarding the geometry and material of the cross section, distribution of the electric field, and the location of smart materials, such as embedded or surface mounted. Several examples have been used to validate the accuracy of the present theory and the resulting code with available results in the literature and the 3D multiphysics simulation using ANSYS.

In addition to the development of a new theory and a new computational tool for modeling slender structures made of smart materials, this paper for the first time clearly and rigorously demonstrates that the variational asymptotic beam sectional analysis (VABS) directly falls out of the Hamilton's principle for elastodynamics of a 3D continuum.

Acknowledgments

This work was supported in part by the Army Research Office under grant 49652-EG-II with Drs. Gary Anderson and Bruce LaMattina as the technical monitors, by the Georgia Tech Vertical Lift Research Center of Excellence, and by the Space Dynamics Laboratory. The views and conclusions contained herein are those of the authors and should not be interpreted as necessarily representing the official policies or endorsement, either expressed or implied, of the funding agencies. The authors also want to thank Drs. Cesnik and Palacios at University of Michigan for the use of UM/VABS.

References

Altay, G.A., Dokmeci, M.C., 2003. Some comments on the higher order theories of piezoelectric, piezothermoelastic and thermopiezoelectric rods and shells. International Journal of Solids and Structures 40, 4699–4706.

Berdichevsky, V.L., 1979. Variational-asymptotic method of constructing a theory of shells. PMM 43 (4), 664–687.

Cesnik, C.E.S., Ortega-Morales, M., 2001. Active beam cross-sectional modeling. Journal of Intelligent Material Systems and Structures 12 (7), 483–496.

Cesnik, C.E.S., Palacios, R., April 2003. Modeling piezocomposite actuators embedded in slender structures. In: Proceedings of the 11th AIAA/ASME/ AHS Adaptive Structures Conference. AIAA, Norfolk, VA.

Cesnik, C.E.S., Shin, S.-J., 2001. On the modeling of integrally actuated helicopter blades. International Journal of Solids and Structures 38 (10–13), 1765–1789.

Chee, C.Y.K., Tong, L., Steven, G.P., 1998. A review on the modelling of piezoelectric sensors and actuators incorporated in intelligent structures. Journal of Intelligent Material Systems and Structures 9, 3–19.

Chopra, I., 2002. Review of state of art of smart structures and integrated systems. AIAA Journal 40 (11), 2145–2187.

Crawley, E.F., Anderson, E.H., 1990. Detailed modeling of piezoceramic actuation of beams. Journal of Intelligent Material Systems and Structures 1 (1), 4–25.

Danielson, D.A., Hodges, D.H., 1987. Nonlinear beam kinematics by decomposition of the rotation tensor. Journal of Applied Mechanics 54 (2), 258–262.

Dong, S.B., Kosmatka, J.B., Lin, H.C., 2001. On Saint–Venant's problem for an inhomogeneous, anisotropic cylinder—Part I: methodology for Saint–Venant solutions. Journal of Applied Mechanics 68, 376–381.

Ghiringhelli, G.L., Masarati, P., Mantegazza, P., 1997. Characterisation of anisotropic non-homogeneous beam sections with embedded piezoelectric materials. Journal of Intelligent Materials, Systems and Structures 8, 842–858.

Giavotto, V., Borri, M., Mantegazza, P., Ghiringhelli, G., Carmaschi, V., Maffioli, G.C., Mussi, F., 1983. Anisotropic beam theory and applications. Computers and Structures 16 (1–4), 403–413.

Han, D., Yu, W., Roy, S., 2007. A geometrically exact active beam theory for multibody dynamics simulation. Smart Materials and Structures 17 (4), 1136–1147.

Hodges, D.H., 2006. Nonlinear Composite Beam Theory. AIAA, Washington, DC.

Le, K.C., 1999. Vibrations of Shells and Rods, 1st ed. Springer, Germany.

Noor, A.K., Venneri, S.L., Paul, D.B., Hopkins, M.A., 2000. Structures technology for future aerospace systems. Computers & Structures 74, 507–519.

Palacios, R., Cesnik, C.E.S., 2005. Cross-sectional analysis of nonhomogeneous anisotropic active slender structures. AIAA Journal 43 (12), 2624–2638.

Park, C., Walz, C., Chopra, I., 1996. Bending and torsion models of beams with induced-strain actuators. Smart Materials and Structures 5 (1), 98–113.

Raja, S., Rohwer, K., Rose, M., 2000. Piezothermoelastic modeling and active vibration control of laminated composite beams. Journal of Intelligent Material Systems and Structures 10, 890–899.

Reddy, J.N., Cheng, Z.Q., 2001. Three-dimensional solutions of smart functionally graded plates. Journal of Applied Mechanics 68 (2), 234–241.

Robbins, D.H., Reddy, J.N., 1991. Analysis of piezoelectrically actuated beams using a layerwise displacement theory. Computers & Structures 41 (2), 265–279.

Saravanos, D., Heyliger, P.R., 1995. Coupled layerwise analysis of composite beams with embedded piezoelectric sensors and actuators. Journal of Intelligent Material Systems and Structures 6 (3), 350–363.

Saravanos, D.A., Heyliger, P.R., 1999. Mechanics and computational models for laminated piezoelectric beams, plates, and shells. Applied Mechanics Review 52 (11), 305–319.

Smyser, C.P., Chandrashekhara, K., 1997. Robust vibration control of composite beams using piezoelectric devices and neural networks. Smart Materials and Structures 6 (2), 178–189.

Taciroglu, E., Liu, C.W., Dong, S.B., Chun, C.K., 2004. Analysis of laminated piezoelectric circular cylinders under axisymmetric mechanical and electrical loads with a semi-analytic finite element method. International Journal of Solids and Structures 41, 5185–5208.

Yu, W., 2002. Variational asymptotic modeling of composite dimensionally reducible structures. PhD thesis, Georgia Institute of Technology.

Yu, W., Hodges, D.H., Volovoi, V.V., Cesnik, C.E.S., 2002. On Timoshenko-like modeling of initially curved and twisted composite beams. International Journal of Solids and Structures 39 (19), 5101–5121.

Zhang, X.D., Sun, C.T., 1996. Formulation of an adaptive sandwich beam. Smart Materials and Structures 5 (6), 814–823.